The Plant Cell, Vol. 26: 2962–2977, July 2014, www.plantcell.org

The Boron Efflux Transporter ROTTEN EAR Is Required for Maize Inflorescence Development and Fertility[C][W][OPEN]

Mithu Chatterjee,[a,1] Zara Tabi,[b,1] Mary Galli,[a] Simon Malcomber,[c,d] Amy Buck,[b] Michael Muszynski,[e] and Andrea Gallavotti[a,f,2]

[a] Waksman Institute, Rutgers University, Piscataway, New Jersey 08854-8020
[f] Department of Plant Biology and Pathology, Rutgers University, New Brunswick, New Jersey 08901
[b] Section of Cell and Developmental Biology, University of California San Diego, La Jolla, California 92093-0116
[c] Department of Biological Sciences, California State University Long Beach, Long Beach, California 90840
[d] Division of Environmental Biology, National Science Foundation, Arlington, Virginia 22230
[e] Department of Genetics, Development, and Cell Biology, Iowa State University, Iowa 50011-2156

Although boron has a relatively low natural abundance, it is an essential plant micronutrient. Boron deficiencies cause major crop losses in several areas of the world, affecting reproduction and yield in diverse plant species. Despite the importance of boron in crop productivity, surprisingly little is known about its effects on developing reproductive organs. We isolated a maize (*Zea mays*) mutant, called *rotten ear* (*rte*), that shows distinct defects in vegetative and reproductive development, eventually causing widespread sterility in its inflorescences, the tassel and the ear. Positional cloning revealed that *rte* encodes a membrane-localized boron efflux transporter, co-orthologous to the *Arabidopsis thaliana* BOR1 protein. Depending on the availability of boron in the soil, *rte* plants show a wide range of phenotypic defects that can be fully rescued by supplementing the soil with exogenous boric acid, indicating that *rte* is crucial for boron transport into aerial tissues. *rte* is expressed in cells surrounding the xylem in both vegetative and reproductive tissues and is required for meristem activity and organ development. We show that low boron supply to the inflorescences results in widespread defects in cell and cell wall integrity, highlighting the structural importance of boron in the formation of fully fertile reproductive organs.

INTRODUCTION

Plant development depends on constant and complex interactions between genetic and environmental factors. To ensure successful reproduction, plants must adapt their growth by sensing and responding to continuous changes in the surrounding conditions, among which is the availability of nutrients in the soil. Nutrients are commonly categorized as macro- or micronutrients depending on whether large or small quantities are required for growth. They generally serve a number of functions in the cell, either as regulators of the electrochemical balance, as cofactors for enzymes, and/or as structural components (Baxter, 2009).

Among the micronutrients, the metalloid boron, naturally present in the soil as boric acid (H_3BO_3) or borate ($H_3BO_4^-$) depending on the pH, has a relatively low natural abundance (Argust, 1998). Because the symptoms of boron deficiency are very diverse and are often attributed to secondary effects (Shorrocks, 1997), it has been a challenge to determine the specific roles of boron in plant development. Most studies of boron have focused on its role in cell wall formation. The pectic polysaccharide rhamnogalacturonan II (RG-II), a highly conserved structural component in plant cell walls (Caffall and Mohnen, 2009), has been shown to cross-link via borate-diol ester bonds and to be necessary for plant growth (Kobayashi et al., 1996; O'Neill et al., 2001). Under conditions of boron deprivation, a decrease in RG-II dimerization has been shown to alter cell wall structure (Findeklee and Goldbach, 1996; Fleischer et al., 1999). Further hypotheses regarding the function of boron in plants propose that the micronutrient could act directly as a signaling molecule, a stabilizer of the plasma membrane, or be involved in auxin metabolism (Loomis and Durst, 1992; Wimmer et al., 2009; Camacho-Cristóbal et al., 2011). A wider role for boron in plants is supported by increasing evidence from vertebrates and eubacteria that boron may also play a role during development in these species (Lanoue et al., 1998; Rowe and Eckhert, 1999; Chen et al., 2002; Fort, 2002).

Plants rely on complex homeostasis networks to regulate the uptake, mobilization, distribution, and storage of micronutrients to assure proper growth (Hänsch and Mendel, 2009). Boron in the soil is acquired via three different routes: diffusion as uncharged boric acid under conditions of adequate or high boron supply; active uptake, predominantly in low boron conditions; and facilitated diffusion through channel proteins (Wimmer and Eichert, 2013). Major breakthroughs in the mechanistic understanding of boron transport were first achieved in *Arabidopsis thaliana*. The *bor1-1* mutant showed increased sensitivity to boron deficiency and reduced boron content in leaves and inflorescences (Noguchi

[1] These authors contributed equally to this work.
[2] Address correspondence to agallavotti@waksman.rutgers.edu.
The author responsible for distribution of materials integral to the findings presented in this article in accordance with the policy described in the Instructions for Authors (www.plantcell.org) is: Andrea Gallavotti (agallavotti@waksman.rutgers.edu).
[C] Some figures in this article are displayed in color online but in black and white in the print edition.
[W] Online version contains Web-only data.
[OPEN] Articles can be viewed online without a subscription.
www.plantcell.org/cgi/doi/10.1105/tpc.114.125963

et al., 1997). *BOR1* encodes a boron efflux transporter whose major function is to export boron out of root tissue and into the xylem for delivery to the shoots (Takano et al., 2002). Other important players in boron transport include members of the Major Intrinsic Protein superfamily. Among these, NOD26-LIKE MAJOR INTRINSIC PROTEIN5;1 (NIP5;1) is a boric acid channel protein that was shown to facilitate boron uptake from the soil into the root (Takano et al., 2006). The combined activity of BOR1 and NIP5;1 represents a two-step process by which boron is absorbed from the soil and transported into the xylem for translocation to the shoot (Miwa and Fujiwara, 2010). *NIP5;1* and BOR1 are transcriptionally and posttranscriptionally regulated, respectively, by boron availability to ensure a tight control of boron uptake that is necessary to avoid problems of toxicity or deficiency (Takano et al., 2005, 2006; Miwa and Fujiwara, 2010). After reaching the shoot, boron is also redistributed, although this process is less understood (Takano et al., 2001). *Arabidopsis* BOR1 and NIP5;1 are members of multigene families, whose individual members contribute both specialized and redundant roles for boron transport (Miwa et al., 2007, 2013).

The inability to take up sufficient amounts of the metalloid due to poor soil quality has become a major agricultural problem in several parts of the world (Shorrocks, 1997), and often crops grown on soil with low boron show reductions in yield and fruit quality (Dell and Huang, 1997). For this reason, much interest has been placed on the possibility of engineering plants that can grow in conditions of boron deficiency or toxicity or on exploiting naturally occurring accessions (Miwa et al., 2006, 2007; Sutton et al., 2007). A detailed account of the effects of boron deficiency in maize (*Zea mays*) was first reported in 1936 and described the disintegration of parenchyma cells in leaves and stems (Eltinge, 1936). In a more recent study monitoring the effects of boron deficiency during maize growth in a controlled setting, growth suppression of both male and female floral organs as well as a decrease in the quantity and the germination frequency of pollen grains were observed (Lordkaew et al., 2011). In a similar study in wheat (*Triticum aestivum*), analogous results were obtained with plants grown in boron-deficient conditions (Huang et al., 2000). How boron limitations cause such symptoms in reproductive development has yet to be determined.

Here, we present a maize mutant called *rotten ear* (*rte*) that is affected in the transport of boron. *rte* mutant plants show major defects in the development and fertility of inflorescences, whereas vegetative defects appear evident only when soil boron concentrations are low. Exogenous application of increasing concentrations of boron resulted in partial to full rescue of both vegetative and reproductive phenotypes and enabled detailed analysis of the developmental consequences of insufficient boron levels. Positional cloning of *rte* and phylogenetic analysis identified the causative locus as a co-ortholog of the *Arabidopsis BOR1* gene. Electron microscopy of *rte* inflorescences revealed defects in meristem and organ development and in the overall integrity of cells and cell walls, suggesting that boron is a major structural component required for maize inflorescence development.

RESULTS

The *rte* Mutant Is Impaired in Tassel and Ear Development

rte is a recessive mutant originally identified in a series of ethyl methanesulfonate (EMS)-mutagenized M2 populations. Among the M2 families analyzed, a single complementation group of recessive mutants displaying small, sterile ears with a brown or "rotten" appearance at the tip and sterile tassels were designated as *rotten ear* (*rte*) (Figure 1). Detailed phenotypic characterization of both tassel and ear was performed on two *rte* alleles (hereafter referred to as *rte-1* and *rte-2*) and in different genetic backgrounds, revealing a range of phenotypic severity imparted by both these factors.

Wild-type maize tassels produce several primary branches that grow from the base of the central spike (Figure 1A). These branches, together with the central spike, each carry a large number of spikelets, enclosed by two glumes, which contain the male florets responsible for pollen production (Supplemental Figure 1). *rte-1* mutant plants in the Mo17 background showed severe defects in tassel development, harboring tassels that were shorter, less branched, and often completely devoid of spikelets (Figures 1B and 1E). However, the severity of these defects was influenced by the genetic background. For example, *rte-1* tassels in the standard inbred line A619 showed a relatively normal number of branches and spikelets, although these spikelets produced only rudimentary organs and no pollen (Figure 1D). A similar, less severe tassel phenotype was also observed in the same background with the *rte-2* allele, whose spikelets appeared to develop all of the basic organs of the male florets—lemma, palea, lodicule, and stamens (Supplemental Figure 1)—but produced little to no pollen.

Analogous phenotypic defects were also observed in the female reproductive organs of *rte* mutants. Wild-type maize ears normally produce multiple rows of spikelets, each containing florets that eventually produce the silks and female gametophytes (Figure 1F). In the Mo17 background, ears of *rte-1* mutants were dramatically reduced in size relative to the wild type (3.6 cm $\pm$ 1.4 versus 27.6 cm $\pm$ 1.7 in the wild type; $n = 10$, $P < 0.0001$), appeared shrunken and withered, and produced no mature spikelets (Figure 1G). A similar but somewhat less pronounced ear phenotype was also observed with the *rte-1* allele in the A619 background (Figure 1H). In these plants, several spikelets developed beyond the meristem initiation stage but were nonetheless infertile. The *rte-2* allele in the A619 background also produced mature spikelets, with the "rotten" phenotype affecting only a small portion of the ear tip (Figure 1I). However, while female florets and silks developed in these samples, the ears of *rte-2* remained sterile, as seen with the *rte-1* allele.

An additional inflorescence-related phenotype comprising clusters of ears emerging from a single leaf axil was also observed. Normally one maize ear is borne at the tip of a short lateral branch, made of several compressed internodes, each carrying quiescent secondary axillary buds. In *rte-1* mutants in both Mo17 and A619 backgrounds, several ears developed on these internodes due to the activation of secondary axillary buds (Supplemental Figure 1). This phenotype is reminiscent of loss of apical dominance in lateral branches.

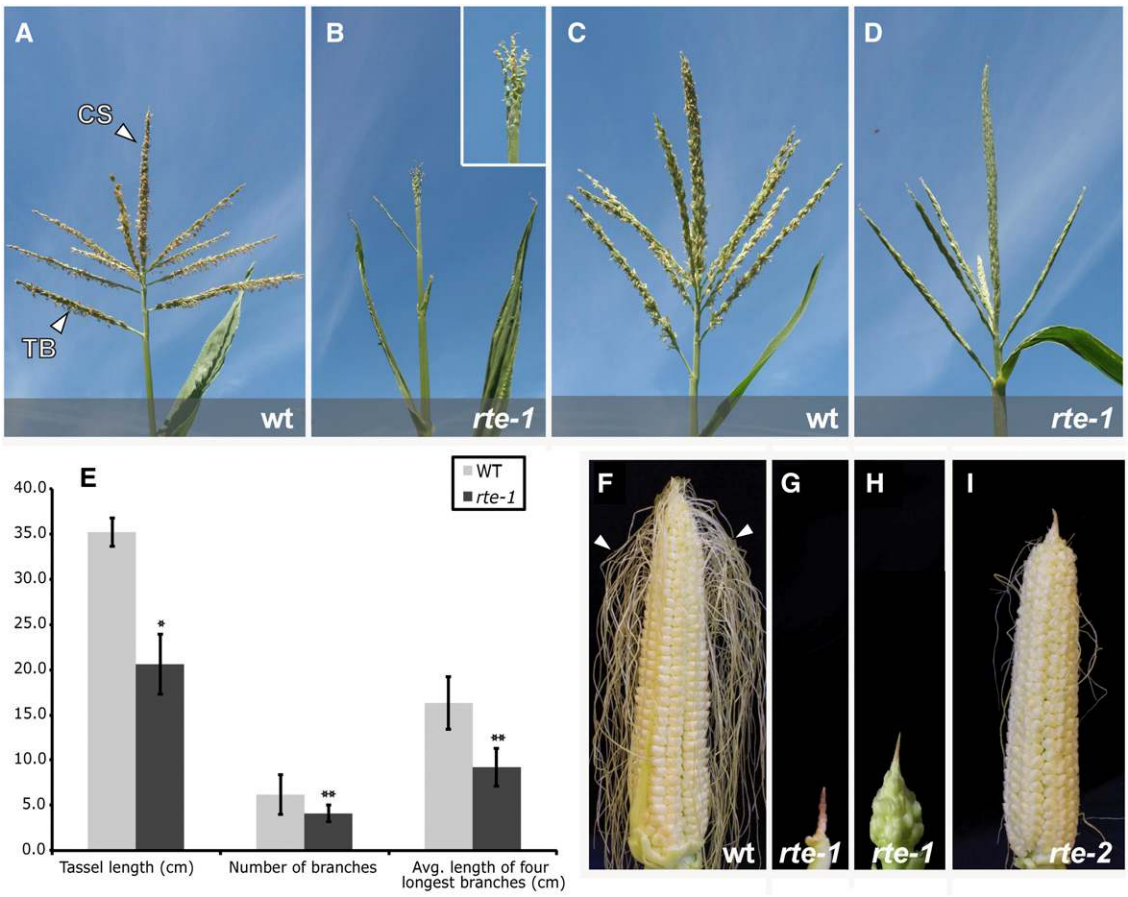

Figure 1. The *rte* Mutant Is Affected in Tassel and Ear Development.

(A) to **(D)** Wild-type and *rte-1* tassels in two different genetic backgrounds, Mo17 (**[A]** and **[B]**) and A619 (**[C]** and **[D]**). CS, central spike; TB, tassel branch.

(E) Quantitative measurements of tassel defects in *rte-1* in the Mo17 background. *t* test, *P < 0.0001; *t* test, **P < 0.05; *n* = 9. Error bars indicate SD.

(F) Wild-type fertilized ear. Arrowheads point to mature silks.

(G) to **(I)** *rte-1* and *rte-2* ears. The majority of the silks have been removed to show the overall ear architecture. In **(G)** and **(H)**, two representative *rte-1* ears in Mo17 and A619 backgrounds, respectively, are shown. In **(I)**, *rte-2* mutant ear in the A619 background showing a shriveled inflorescence tip and sterile florets.

Vegetative phenotypes were also occasionally observed in *rte* mutants. After the transition to reproductive development, emerging leaves showed necrotic lesions, were reduced in size, and looked discolored and wrinkly. Saffranin-O/Alcian Blue staining of leaf cross sections in these areas revealed a loss of regularly arranged vascular bundles and the presence of highly lignified tissue (Supplemental Figure 2).

In addition to the influences imparted by different genetic backgrounds and alleles, further variations in the severity of both vegetative and inflorescence phenotypes were frequently observed with all *rte* mutants, suggesting an environmental effect on the observed developmental defects. Regardless, all *rte* alleles were completely sterile under all conditions evaluated, producing neither viable pollen nor fertile ears, and self-crosses of mutants as well as outcrosses were always unsuccessful.

In order to investigate in detail the basis of these defects, we focused on the female inflorescence where the *rte* phenotype was most consistent and severe. Wild-type maize ears develop as a result of multiple rows of axillary meristems with different identities and fates originating on the flanks of a central inflorescence meristem (McSteen et al., 2000). These meristems are named according to the structure that they form: spikelet-pair meristems (SPMs) form pairs of spikelets, spikelet meristems (SMs) form spikelets, and floral meristems form florets (Figure 2). Eventually mature florets capable of producing elongated silks receptive to pollen are formed (Figures 1F and 2F). This growth pattern proceeds acropetally. Scanning electron microscopy images of young ear primordia (Figure 2) showed that *rte* mutant ears were nearly indistinguishable from wild-type ears at the early stages of development and that SPMs and SMs were correctly formed at the flanks of the inflorescence meristem (Figures 2A, 2B, 2G, and 2H). However, as ear development progressed and the "rotten" phenotype manifested itself toward the tip, newly forming SPMs, SMs, and floral meristems, as well as the inflorescence meristem itself appeared malformed and

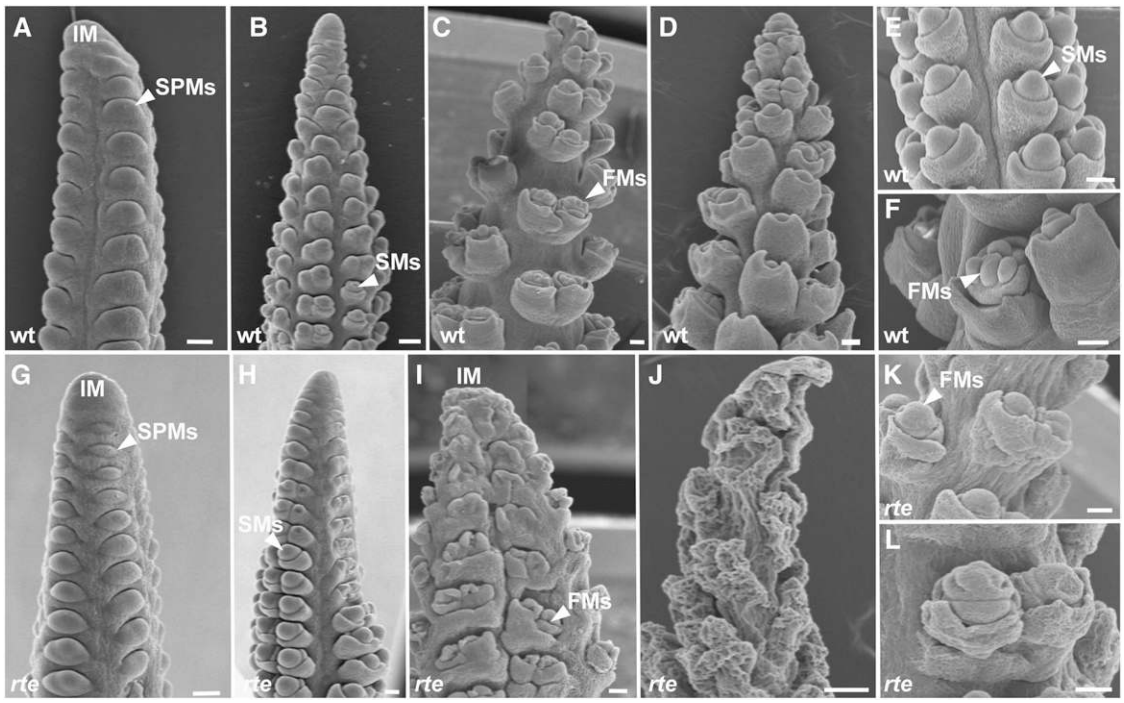

Figure 2. Scanning Electron Microscopy Analysis of Immature *rte* Ears.

(A), **(B)**, **(G)**, and **(H)** In the early stages of ear primordia development, no visible differences are noted between wild-type (**[A]** and **[B]**) and *rte* (**[G]** and **[H]**) ears at 0.5 and 1.5 cm length.

(C) to **(F)** and **(I)** to **(L)** Later in development (>2 cm), clear differences can be seen between the wild type (**[C]** to **[F]**) and the *rte* mutant (**[I]** to **[L]**). The *rte* phenotype is particularly evident in the ear tip where the inflorescence meristem collapses, floral meristems and floral organs appear malformed **(I)**, and the overall tissue eventually wrinkles (**[J]** to **[L]**).

FMs, floral meristems. Bars = 100μm.

withered (Figures 2C to 2F and 2I to 2L; Supplemental Figures 3A and 3E). This analysis confirmed that it is the later stages of inflorescence development that are predominantly impaired in *rte* mutants. Further scanning electron microscopy analysis revealed withering of the cob tissue that supports the growing reproductive meristems (Figures 2E and 2K), suggesting an overall weakening of the entire inflorescence structure.

The lack of visible developmental and molecular defects in early stages of reproductive organ formation indicates that *rte* mutants are not impaired in axillary meristem initiation per se, but rather fail to maintain growth of meristems and developing organs. In situ hybridizations with the meristem maintenance marker *knotted1* (*kn1*) (Jackson et al., 1994) showed normal *kn1* expression in most meristematic tissues of developing *rte* ears, indicating that the *rte* mutant can successfully initiate axillary meristems at the initial stages (Supplemental Figure 4A). However, as ear development progressed the inflorescence meristem did not maintain the strong level of *kn1* expression that was typically observed in wild-type plants (Supplemental Figure 4B). This suggests that the *rte* gene plays a role in maintaining meristematic identity or that *kn1* expression is simply lost once the inflorescence tip starts to degenerate. Taken together, these findings suggest that *rte* mutants fail to sustain growth of rapidly dividing meristematic tissues and developing organs, presumably due to cell expansion defects.

Toluidine blue-stained sections of wild-type and *rte-1* ears revealed that developing spikelets and florets of *rte-1* appeared to initially shrink and eventually collapse during later developmental stages (Supplemental Figure 3). Further sections of developing meristems showed wrinkled surface tissue and a widespread loss of internal cellular organization. In agreement with the scanning electron microscopy analysis, these observations suggest that *rte-1* mutants are not capable of sustaining meristem and organ growth. Furthermore, the sterility of *rte* ears is likely caused by the collapse of the floral meristem and floral organs, rather than by any specific defects in *rte-1* silk development, which morphologically resembled wild-type silks (Supplemental Figure 3).

rte Encodes a Putative Boron Transporter

In order to identify the gene responsible for the *rte* mutant phenotype, we first generated M3 mapping populations from the original M2 families. Using these populations, we preliminary mapped four *rte* mutants by bulk segregant analysis using a high-throughput SNP-genotyping platform (Liu et al., 2010). All *rte* mutants mapped to the same region on the upper arm of chromosome 1 in bin 1.05 (Figure 3A). The preliminary map position was subsequently confirmed through the use of simple sequence repeat (SSR) markers that defined the genetic interval encompassing the *rte* locus between SSR markers umc1076 and umc2232 (Figure 3A).

A total of 319 mutant plants from an M3 population segregating the *rte-1* allele were used to narrow the *rte* locus to a 3.2-Mb region between markers MAGIv4_1364 and MAGIv4_55889 (Figure 3A; Supplemental Table 1). We compared our mapping region to the corresponding syntenic region in sorghum (*Sorghum bicolor*) and found it spanned a 0.68-Mb interval on chromosome 8. We analyzed the sorghum sequence in this interval and identified 33 predicted genes (Figure 3A) that were used to find the corresponding maize genes. One of the candidate genes that fell within the mapping window encoded a putative transporter, *GRMZM2G166159* (Figures 3A and 3B), with high amino acid similarity to the *Arabidopsis* boron efflux transporter BOR1 (Takano et al., 2002). Sequencing of this gene in *rte-1* mutants revealed a cytosine deletion at position +330 of the coding sequence, which resulted in a frameshift (Figure 3B). Sequencing of this same gene in *rte-2*, detected a single nucleotide change at position +1078, which produced a premature stop codon (CAA to TAA). Subsequently, we sequenced two additional alleles, *rte-3* and *rte-4* (Supplemental Figure 5). *rte-3* contained a premature stop codon (TGG to TGA at +739 position), whereas *rte-4* contained a single nucleotide change (TCA to TTA) that resulted in the substitution of a highly conserved serine residue to a leucine (S361L) (Figure 3B; Supplemental Figure 6). The occurrence of four different, independent lesions in the coding sequence of *GRMZM2G166159* demonstrates that this locus corresponds to the *rte* gene (Figure 3B).

Boron Application Rescues the Phenotypic Defects of *rte* Mutants and Restores Fertility

To independently verify that the *rte* phenotype was caused by defective boron supply from the root to the shoot, we sought to rescue the developmental defects with exogenous application of boron. Homozygous *rte-1* mutants and heterozygous siblings were grown under standard greenhouse conditions and irrigated with five increasing concentrations of boric acid (20, 100, 200, 500, and 1000 μM) or water alone. Vegetative and reproductive defects were then monitored at these concentrations (Figure 4). Little to no phenotypic rescue of *rte* mutants was observed at boric acid concentrations below 100 μM or with water alone; however, partial rescue became apparent at 100 μM boric acid. Specifically, widespread leaf lesions typically appearing on the

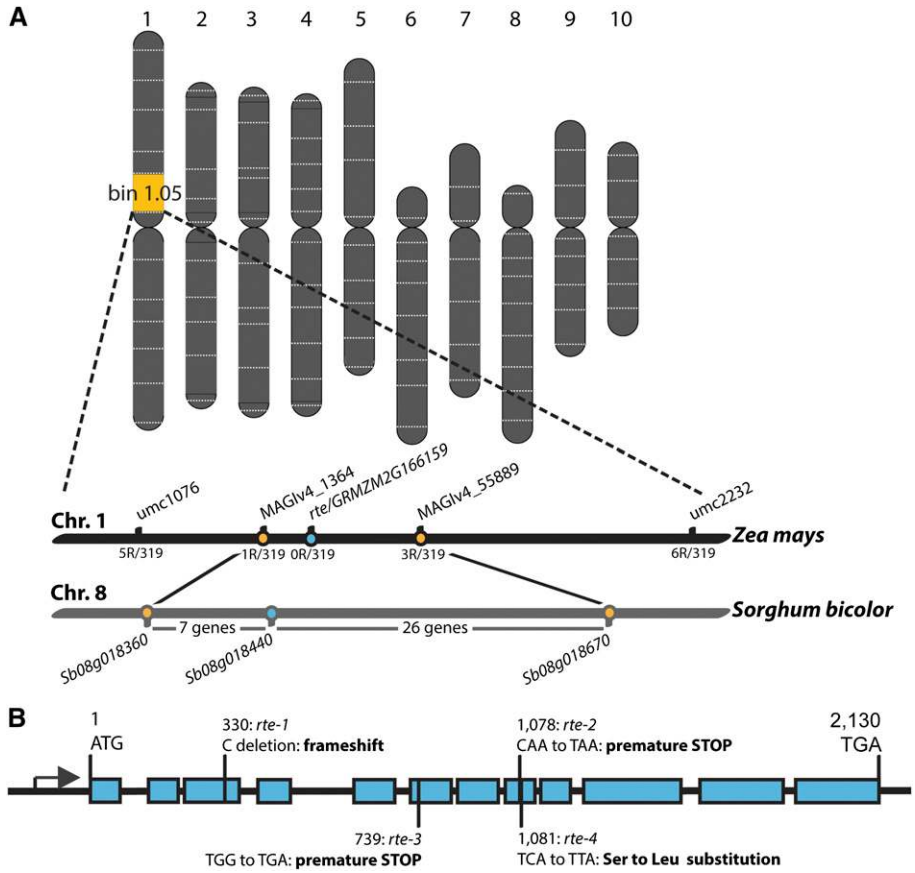

Figure 3. Positional Cloning of *rte.*

(A) Schematic representation of the map-based cloning of the *rte* gene located on chromosome 1.
(B) *rte* gene structure and location of mutant alleles. Rectangles represent exons, and the black arrow represents the transcription start site.
[See online article for color version of this figure.]

fifth and all subsequent fully developed leaves of *rte-1* plants were no longer observed on the rescued plants (Figures 4B, 4D, and 4F) and the tassels began to produce several fertile spikelets (Figure 4E; Supplemental Figure 7) containing viable pollen grains (Figures 4H and 4I). Pollen from these plants was successfully used to fertilize nonmutant ears (Figure 4G). In order to restore female fertility, a higher supplemental boron concentration than that needed in the tassel was required. While 100 μM boric acid resulted in more developed ear structures (Figure 4L) relative to those seen at lower concentrations (Figure 4K) and even produced wild-type-looking silks, no fertilized kernels were produced in several crossing attempts with wild-type pollen (n = 5). Complete rescue of the *rte-1* ear phenotype and fertility defects were obtained at 200 μM boric acid (Figure 4M). This higher

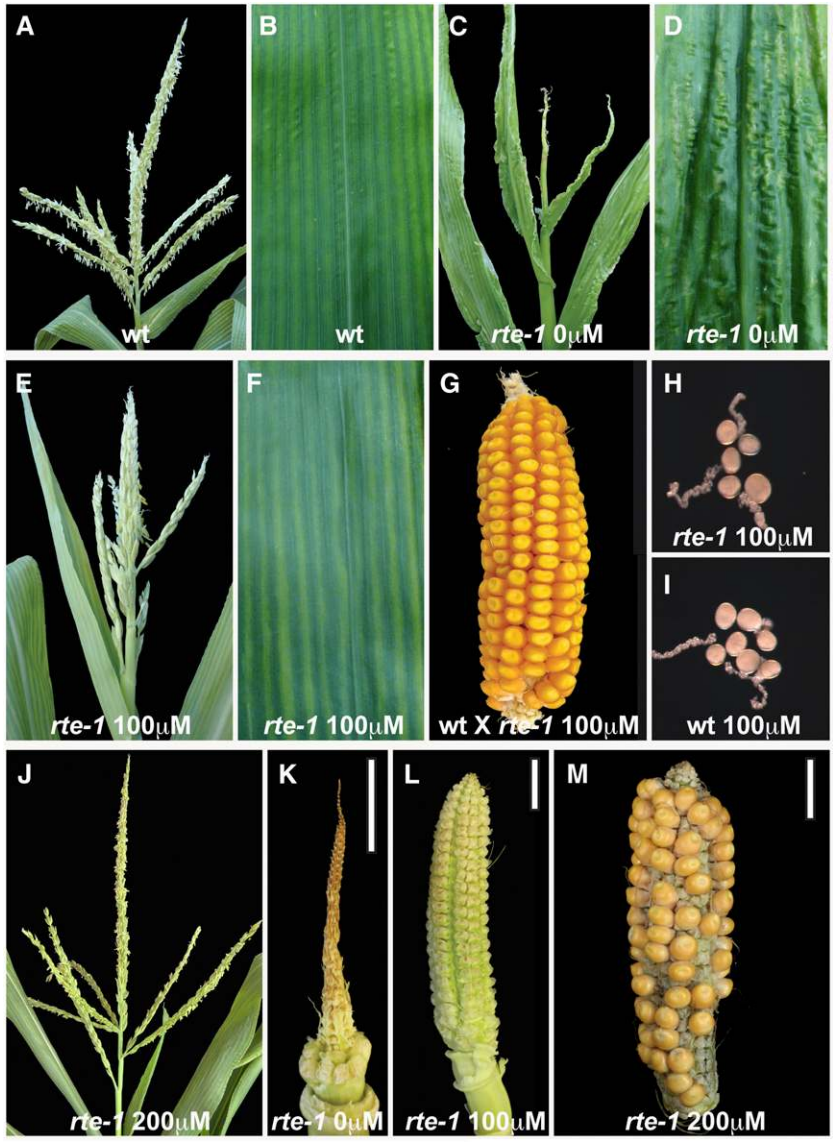

Figure 4. Rescue of the *rte* Phenotype by Exogenous Boric Acid Application.

(A), **(C)**, **(E)**, and **(J)** Tassels of wild-type and *rte-1* plants at different boric acid concentrations.
(B), **(D)**, and **(F)** Leaves of wild-type and *rte-1* plants at different boric acid concentrations.
(G) Successful fertilization of a wild-type ear using pollen from an *rte-1* tassel treated with 100 μM boric acid.
(H) and **(I)** Fertile pollen grains in pollen germination media from *rte-1* plants rescued with 100 μM boric acid **(H)** and fertile pollen grains from the wild type **(I)**.
(K) and **(L)** Ears from *rte-1* plants grown in different boric acid concentrations.
(M) Successful cross obtained using an ear from a *rte-1* plant treated with 200 μM boric acid and wild-type pollen.
Bars = 2 cm.

concentration of boric acid also resulted in the full restoration of the *rte-1* tassel phenotype to a wild-type appearance (Figure 4J; Supplemental Figures 7 and 8). Similar rescue of *rte-1* reproductive defects was obtained with plants grown at 500 and 1000 μM boric acid. At all supplemental boric acid concentrations, heterozygous *rte* control plants maintained a wild-type appearance, indicating that our conditions were not toxic to normal maize plants. Overall, these results demonstrate that the *rte* mutant phenotype can be rescued by the exogenous application of boron and highlights the importance of RTE for the transport of boron into developing inflorescences.

The Severity of the *rte* Phenotype Correlates with Boron Concentrations in the Soil

As previously mentioned, we observed that the phenotypic severity of field-grown *rte-1* mutants appeared to be influenced by genetic as well as environmental factors related to where the plants were grown. Over the course of our experiments, identical *rte-1* genetic material (*rte-1*, backcrossed to Mo17) was grown in three different locations: the University of California San Diego (UCSD) field station in La Jolla, CA, during the summer of 2011; the Rutgers University Horticultural field station in East Brunswick, NJ, in summer 2012; and the Hawaiian Research field station in Molokai, HI, during the winters of 2009 and 2012. A severe *rte* phenotype was observed in both the UCSD and Rutgers fields, while in the Molokai field, the same allele showed a much milder phenotype in two separate years (Supplemental Figure 9). Both tassels and ears, despite appearing well formed and containing a normal number of branches and spikelets, were nonetheless sterile at the Molokai location. Given that *rte* encodes a boron transporter, we checked if the phenotypic variation observed in field-grown plants could be attributed to different naturally occurring concentrations of boron in the soil. Soil samples taken from the field in Molokai showed significantly higher boron concentrations than soil samples taken from both the UCSD and Rutgers fields, 2.35 ppm versus 1.14 ppm and 0.39 ppm, respectively. These concentrations correlated with the reduced severity of the *rte-1* phenotype in the boron-rich soil of Molokai and the stronger phenotypes observed in the relatively boron-poor soils of UCSD and Rutgers (Supplemental Figure 9). Furthermore, at Rutgers, where the lowest concentration of boron in the soil was detected (0.39 ppm), we observed both strong inflorescence and leaf phenotypes (Supplemental Figure 9). Leaf phenotypes were also noted at the UCSD field, although not consistently, and were never observed at the Molokai fields (Supplemental Figure 9). Nevertheless, measurements of leaf boron levels of Molokai-grown *rte* mutants were 20 to 30% lower relative to the wild type (a difference similar to that found in ears; Supplemental Figure 10), indicating defective boron transport of *rte* mutants even in relatively boron-rich soils. These findings emphasize the effects of naturally occurring soil boron concentrations on the *rte* phenotype and the necessity for a dynamic boron transport system for naturally occurring variation in B availability.

rte Is Co-Orthologous to the *Arabidopsis* Boron Transporter *BOR1*

Comparative sequence analysis revealed that RTE shares 80% amino acid identity and 90% similarity with the *Arabidopsis* boron efflux transporter BOR1 (Takano et al., 2002). Bayesian phylogenetic analysis on a collection of RTE-related proteins from a sample of land plants placed the maize *rte* gene within a strongly supported clade (1.00 posterior probability) with the *Arabidopsis BOR1* (*At2g47160*) locus (Figure 5). Within this clade were two large eudicot subclades that were sister to a monocot-exclusive subclade (Figure 5, blue), suggesting that a duplication event within this lineage had occurred near the base of eudicots. Local duplications are also estimated within Brassicaceae, Euphorbiaceae, Fabaceae, and Salicaceae that might suggest local sub- or neofunctionalization within these different lineages. *rte* belongs to a strongly supported monocot subclade (Figure 5, blue) together with another maize locus (*GRMZM2G082203*) and loci from other grass species (*Brachypodium distachyon*, sorghum, and rice [*Oryza sativa*]). The rice locus (Os-*BOR1*; *Os12g37840*) has been previously characterized as a boron transporter and *BOR1* homolog (Nakagawa et al., 2007). The second maize locus, *GRMZM2G082203* (hereafter *rte2*), is sister to the sorghum sequence, and this maize-sorghum clade is in turn sister to *rte* pointing to a gene duplication event within andropogonoid grasses. BLAST searches showed that *rte2* had a 94% nucleotide alignment with *rte*, which translated to 95% amino acid similarity.

To assess if *rte* and *Arabidopsis BOR1* share a similar function during development, we performed a functional complementation test using *Agrobacterium tumefaciens*-mediated transformation of the *Arabidopsis bor1-3* mutant (Kasai et al., 2011) with the maize *rte* gene placed under the control of the 35S promoter. Homozygous *bor1-3* insertion lines grown without supplemental boron showed dark-green dwarfed leaves, reduced apical dominance, and fertility issues that led to a severe reduction in seed set (Figures 6A, 6B, 6E, and 6G). Close examination of the floral defects in these lines revealed that infertility often resulted from the premature withering of the floral organs at various stages of flower development, a phenotype reminiscent of *rte* mutants (Figure 6F). The vegetative defects of homozygous *bor1-3* plants were completely rescued in 26 out of 26 independent lines containing the $35S_{pro}$*:rte* construct, while fertility defects were rescued in ~50% of these lines (Figures 6C and 6H). In contrast, transformation of homozygous *bor1* plants with a construct containing the *rte-4* mutation (S361 to L361; $35S_{pro}$*:rte* L361) resulted in no rescue of either vegetative or reproductive defects in 16 lines examined (Figure 6D). Overall, these results indicate that RTE is a functional co-ortholog of the BOR1 boron efflux transporter.

The *rte* gene encodes a polypeptide of 709 amino acids comprising 10 putative transmembrane domains (Figure 3B; Supplemental Figure 6), similar to *BOR1*. To determine the subcellular localization of the RTE protein, we used a tobacco (*Nicotiana benthamiana*) transient expression assay with a $35S_{pro}$*:rte:YFP* (yellow fluorescent protein) reporter construct. The RTE-YFP fusion protein predominantly localized to the plasma membrane when visualized via confocal microscopy (Figure 6I). Detailed analysis also showed the RTE-YFP fusion protein in putative endosomal compartments. Similar transient expression of a construct containing the *rte-4* S361 to L361 mutation fused to YFP ($35S_{pro}$*:rte L361:YFP*) failed to show strong localization at the plasma membrane as seen for RTE-YFP. Instead, the RTE-L361-YFP fusion protein localized to putative endosomal and other

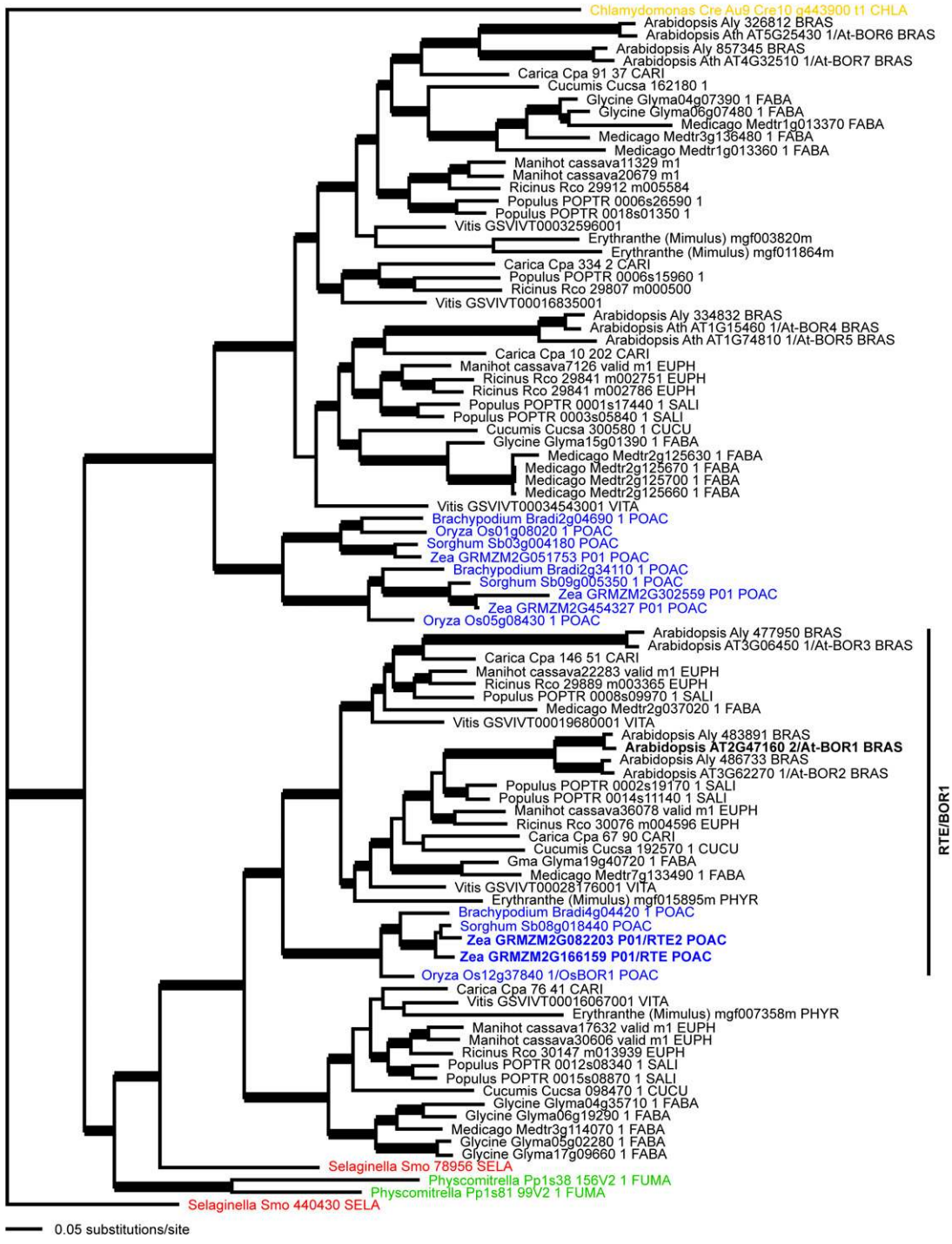

Figure 5. Bayesian Consensus Phylogram of 94 RTE-Like Proteins from Land Plants.

Thick branches indicate ≥95% posterior probability. Black, eudicots; blue, monocots; red, lycophyte; green, mosses; orange, green alga. Taxonomic family abbreviations: BRAS, Brassicaceae; CARI, Caricaceae; CHLA, Chlamydomonaceae; CUCU, Cucurbitaceae; EUPH, Euphorbiaceae; FABA, Fabaceae; FUMA, Fumariaceae; PHYR, Phyrmaceae; POAC, Poaceae; SALI, Salicaceae; SELA, Selaginellaceae; VITA, Vitaceae. Maize Zm-RTE and *Arabidopsis* At-BOR1 are highlighted in bold, and the RTE/BOR1 clade is marked.

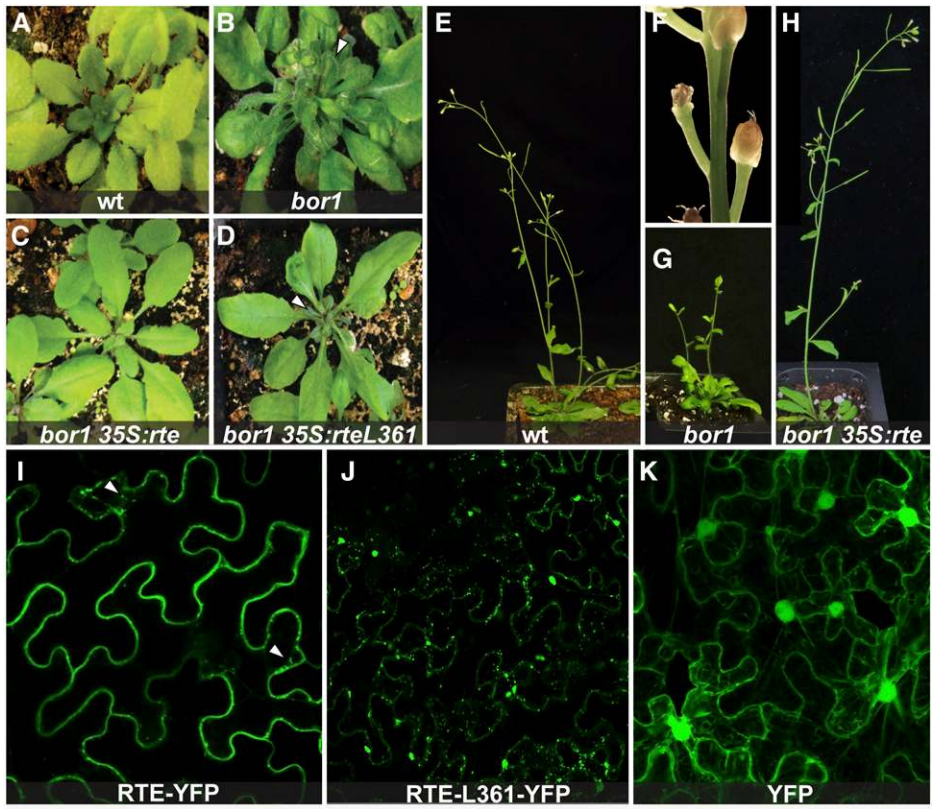

Figure 6. RTE Rescues the *Arabidopsis bor1* Mutant and Localizes to the Plasma Membrane.

(A) to **(D)** The vegetative *bor1-3* phenotype is rescued by the $35S_{pro}$*:rte* construct but not by the $35S_{pro}$*:rte* L361 construct. Arrowheads point to defective leaves.

(E) to **(H)** The reproductive defects of *bor1-3* (reduced apical dominance, floral defects, and infertility) are also rescued by the $35S_{pro}$*:rte* construct. **(F)** is a close-up picture of *bor1-3* flower buds.

(I) to **(K)** Confocal images of RTE-YFP, RTE-L361-YFP, and YFP proteins expressed in tobacco cells. Arrowheads point to putative endosomal compartments.

punctate compartments (Figure 6J). Both localization patterns were in contrast to the signal observed with our $35S_{pro}$*:YFP* control construct, which was homogenously distributed throughout the cell, including the nucleus and the cytosol (Figure 6K). These results show that RTE, like BOR1, is localized to the plasma membrane and is able to undergo endosomal cycling. The altered subcellular localization of the RTE-L361-YFP protein likely explains the failure to rescue the *bor1-3* mutant by the $35S_{pro}$*:rte L361* construct (Figure 6D).

The *rte* Gene Is Primarily Expressed in Vascular Tissue throughout Development

To determine in which tissues the *rte* gene was expressed, quantitative RT-PCR was performed. *rte* mRNA was detected in both vegetative (roots and leaves) and reproductive tissue, showing the highest relative expression levels in immature ears. Lower amounts of transcript were also detected in endosperm and embryos (Figure 7A). This expression profile was in agreement with expression data from a collection of RNA-seq experiments from different maize tissues (Supplemental Figure 11).

To further investigate the specific domain of *rte* expression in vegetative and reproductive tissues, mRNA in situ hybridizations were performed (Figures 7B to 7E). In transverse sections of young maize stems and leaves, strong expression of *rte* was observed primarily in the vasculature (Figures 7B and 7C). More specifically, high expression was seen in the cells surrounding the xylem and the phloem (Figures 7B and 7C). Similar expression patterns were detected in longitudinal sections of developing inflorescences, where strong signal was observed in the vasculature (Figure 7E). Overall, the presence of *rte* transcripts in multiple tissue types suggests that *rte* acts throughout maize development.

Transmission Electron Microscopy Analysis of Developing *rte* Ears Reveals Defects in Cell and Cell Wall Integrity

The primary role of boron in plants is currently believed to be structural, involving the cross-linking of RG-II dimers that influence cell expansion and cell wall thickness and porosity (Miwa et al., 2013; Chormova et al., 2014). Reduced levels of RG-II/B dimers in shoots and roots have been reported for *bor1* and *bor2* mutants, respectively (Noguchi et al., 2003; Miwa et al., 2013). In

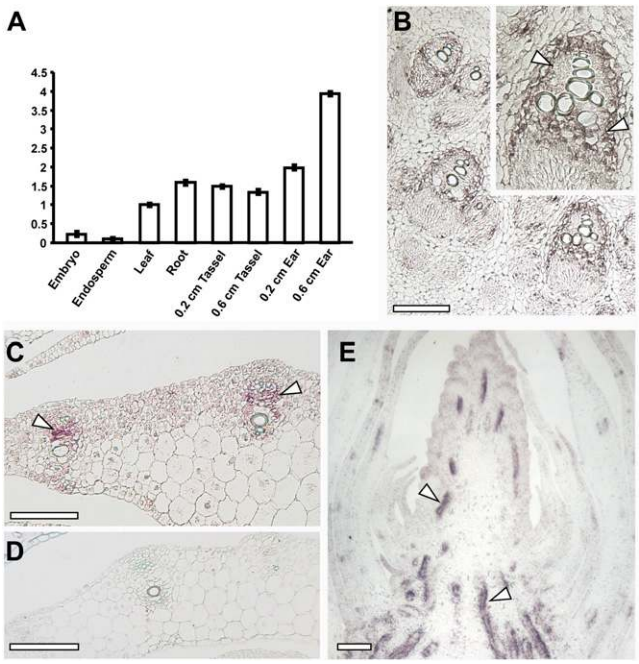

Figure 7. Expression Analysis of *rte.*

(A) Quantitative RT-PCR of *rte* in different maize tissues. The *y* axis shows the fold change relative to leaf expression levels. Error bars in the figure represent SE of the mean.
(B) to **(E)** In situ hybridizations of *rte* in stems, leaves, and inflorescences of wild-type plants.
(B) Cross section of a seedling stem showing *rte* expression in vascular cells. Inset: close-up of a vascular bundle; strong expression is observed in cells surrounding the xylem (arrowheads).
(C) and **(D)** Cross sections of leaves hybridized with *rte* antisense **(C)** and negative control sense probes **(D)**.
(E) Longitudinal section of an immature ear. *rte* transcripts are localized to vasculature (arrowheads).
Bars = 200 μm.

order to assess the cellular consequences of insufficient boron supply in reproductive tissues, we analyzed the ultrastructure of *rte* mutant ears at different developmental stages using transmission electron microscopy (TEM). Cells from ears that did not yet show the *rte* phenotype appeared structurally intact and similar to the wild type (Figures 8A to 8D). At later stages of ear development where the phenotype was apparent at the tip but not yet "rotting," several defects were frequently observed. The cell wall appeared loosened and swollen, and the structural integrity of the cell and organization of the tissue compromised (Figures 8E and 8F). As development progressed, TEM analysis showed that *rte* mutant cells had disintegrated: plasma membranes detached, cell walls disappeared, and overall cell death was observed (Figures 8G and 8H). In summary, the inability of *rte* mutants to properly transport and distribute boron results in visible damage to the cell wall and other cellular components necessary for the development of reproductive organs and supporting tissue, indicating that the primary role of boron in maize inflorescences is to support the structural integrity of cells and cell walls.

DISCUSSION

The Importance of Boron Transport for Maize Development

The ability of plants to acquire adequate amounts of boron from the soil results from the tight regulation of two protein families known to act in boron transport: channel proteins belonging to the NIP family and the BOR family of efflux transporters (Miwa and Fujiwara, 2010). Mutations in both families have been characterized in *Arabidopsis* and rice and result in severe developmental defects (Noguchi et al., 1997; Takano et al., 2006; Miwa et al., 2007, 2013; Nakagawa et al., 2007; Tanaka et al., 2008). While reduced fertility has been reported in these mutants, most studies have focused primarily on roots with limited analysis being dedicated to how these genes affect reproductive development, despite its economic importance.

We identified a novel maize mutant displaying severe inflorescence development phenotypes and established that the causative *rte* locus encodes a functional ortholog of the *Arabidopsis BOR1* boron efflux transporter. Our findings show that *rte* reproductive defects manifest in both male and female inflorescences. Depending on genetic background and environmental conditions, tassels failed to produce branches and spikelets, whereas ears remained small and collapsed at the growing tip (Figure 1). Histological and scanning electron microscopy analysis indicated that these phenotypes resulted from the failure to maintain both inflorescence and axillary meristem activity (Figure 2; Supplemental Figure 3).

Analysis of *rte* mutants at various boron concentrations, either artificially applied or naturally present in the soil, provided a spectrum of phenotypic severity. This allowed the dissection of the various effects of boron deficiency in specific maize developmental processes. The organ most sensitive to *rte*-dependent transport and low boron concentrations was the ear, where the highest expression of the *rte* gene was detected in quantitative RT-PCR analysis (Figure 7A). At 100 μM supplemental boric acid concentrations, *rte* ears formed all reproductive organs but nonetheless were unable to produce kernels when fertilized with wild-type pollen. This situation contrasted with that in male inflorescences where pollen fertility was restored under these conditions. Only at 200 μM boric acid was the appearance and fertility of ears restored. Since the silks appeared to be morphologically normal in *rte* mutants grown under boron-deficient conditions (Supplemental Figure 3), the sterility of *rte* ears is most likely due to the malformation or absence of the female gametophyte caused by the collapse of the floral meristems (Figure 2; Supplemental Figure 3). Alternatively, the silks of *rte* mutants, though morphologically indistinguishable from the wild type, may be nonreceptive. Interestingly, *rte* is highly expressed in both silks and ovules (Supplemental Figure 11) and may therefore perform a specific role in these tissues that could explain the observed female sterile phenotype. The higher sensitivity of the *rte* mutation in ears compared with tassels and leaves may indicate that higher boron concentrations are required for ear development, or it could result from the fact that ears develop later and consequently are the organ most susceptible to the increasingly limited amounts of boron available as *rte* mutants grow in size.

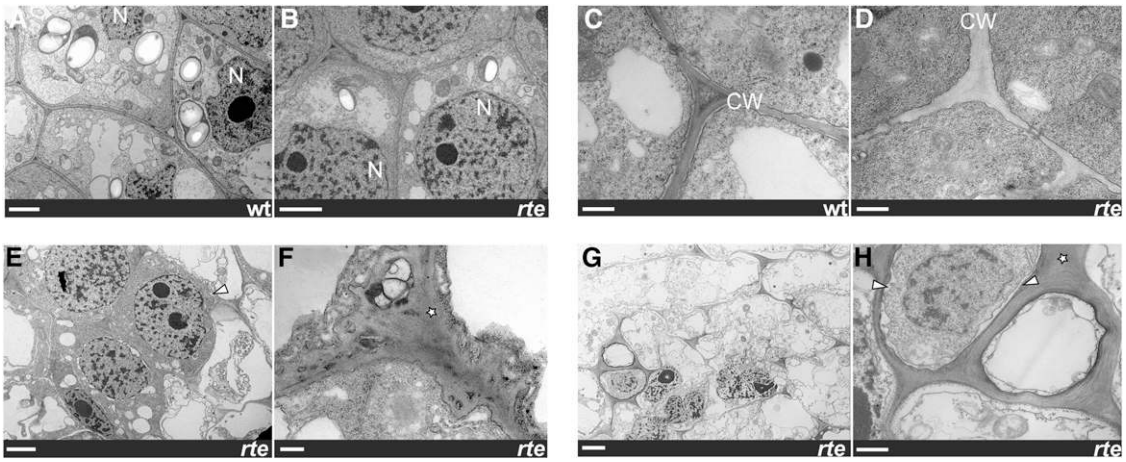

Figure 8. TEM Analysis of *rte* Ears.

Zoomed-out view of cells (**[A]**, **[B]**, **[E]**, and **[G]**) and close-up views of cell walls (**[C]**, **[D]**, **[F]**, and **[H]**) in wild-type and *rte* ears. Stars indicate abnormal and swollen cell walls; arrowheads indicate shrinking cells and plasma membranes. Bars = 2 μm in (**[A]**, **[B]**, **[E]**, and **[G]**) and 0.5 μm in (**[C]**, **[D]**, **[F]**, and **[H]**). N, nucleus; CW, cell wall.

Another intriguing aspect was the formation of ear clusters, presumably resulting from the loss of apical dominance in the lateral branches that give rise to the ears (Supplemental Figure 1). The loss of apical dominance in secondary axillary buds suggests that in *rte* mutants auxin transport is perturbed (Domagalska and Leyser, 2011). This phenotype may be due to the collapse of the main inflorescence meristem in primary ear primordia, an auxin source, causing a lack of lateral inhibition of the secondary axillary buds. A loss of apical dominance is also observed in *bor1* mutants (Noguchi et al., 1997; Figure 6G) and may similarly be caused by altered auxin transport. Alternatively, these auxin-related phenotypes may indicate a direct connection between boron availability and auxin. Interestingly, the relationship between cell wall pectins and auxin transport has recently been investigated in terms of the cellular mechanical changes required for organ formation (Braybrook and Peaucelle, 2013).

RTE Is a Boron Transporter Whose Function Is Conserved in Monocot and Eudicot Species

Phylogenetic and protein sequence analysis show that RTE is co-orthologous to the previously characterized *Arabidopsis* BOR1 efflux carrier (Takano et al., 2002). Analogous to the expression of *AtBOR1* in root pericycle cells (Takano et al., 2002), we observed *rte* expression in cells surrounding the vasculature in vegetative and reproductive tissues. Similarly, the *BOR1*-related rice Os-*BOR1* and barley (*Hordeum vulgare*) *Bot1* genes are also expressed in areas surrounding the vasculature (Nakagawa et al., 2007; Sutton et al., 2007; Pérez-Castro et al., 2012).

rte and At-*BOR1* lie within a strongly supported phylogenetic clade along with other co-orthologous genes from both monocot and eudicot species, some of which were previously characterized as boron transporters (Miwa et al., 2007; Nakagawa et al., 2007). The rescue of the *Arabidopsis bor1* phenotype by overexpression of *rte* indicates that the two genes are functionally homologous. The *bor1* mutant phenotype was also rescued by overexpression of the grape *BOR1* ortholog Vv-*BOR1* (Pérez-Castro et al., 2012). Altogether, these results suggest that the function of this transporter is conserved between eudicots and monocots.

Several elegant studies have revealed how BOR1 is post-transcriptionally regulated in a boron-dependent fashion. When plants are grown in high boron conditions, the BOR1 protein is transported to the endosomal compartment and then to the vacuole for degradation (Takano et al., 2005, 2010; Kasai et al., 2011). BOR1 is also polarly localized to the inner plasma membrane in *Arabidopsis* root cells (Alassimone et al., 2010; Takano et al., 2010; Roppolo et al., 2011). Three tyrosine residues (Y373, Y398, and Y405) located in a large putative cytoplasmic loop were shown to be important for polar localization of BOR1 and its endosomal recycling (Takano et al., 2010; Kasai et al., 2011; Yoshinari et al., 2012). Only Y398 and Y405 are conserved in grasses (Supplemental Figure 6).

We identified one *rte* allele, *rte-4*, that carries a single amino acid substitution in a highly conserved serine residue (S361L; Supplemental Figure 6), located in the same cytoplasmic region as the above-mentioned tyrosine residues. S361 is conserved in all sampled proteins from the BOR1/RTE clade and likely serves an important function. Transient overexpression of RTE-L361-YFP in tobacco resulted in a strikingly different subcellular localization pattern compared with wild-type RTE-YFP or YFP alone. The predominance of RTE-L361-YFP signal in punctate compartments and aggregates supports the importance of this residue for proper cellular trafficking. The polar localization of several transporters is regulated by the reversible phosphorylation of specific serine residues by Ser/Thr kinases (Huang et al., 2010). The S361 residue of RTE could be regulated in a similar fashion. Alternatively, this residue, which is located just after the eighth transmembrane domain (Supplemental Figure 6) (Takano et al., 2010; Yoshinari et al., 2012), may affect the conformation of the protein and interfere with other residues involved in trafficking. The lack of rescue of the *bor1* phenotype by the overexpression

of RTE-L361 is consistent with its lack of membrane localization (Figure 6J) and suggests that the S361 residue may be important in the subcellular localization of RTE proteins.

Our phylogenetic analysis (Figure 5) also revealed that maize harbors a closely related homolog of *rte* (*GRMZM2G082203*), which most likely resulted from a duplication event within andropogonoid grasses. Whether or not this gene is functional is not known, but it is expressed in various maize tissues (http://www.qteller.com). The fact that *rte* mutants grown under conditions of relatively low boron showed a severe phenotype raises the possibility that either the duplicate gene is not functional, or more likely, it is able to only partially compensate for the lack of *rte*. Vegetative defects are only observed in strong *rte* mutant backgrounds and are more evident in soils with low boron content (Supplemental Figure 9). It is therefore possible that the *rte* paralog may be sufficient to sustain growth during the early stages of development in *rte* mutant plants, but as the plants develop, the translocation of boron from the root to the shoot by the *rte* paralog is no longer able to efficiently sustain growth. Therefore, boron-deficient symptoms are more evident in organs that form later in development, such as the tassel and the ear.

A duplication event similar to that seen with maize *rte* is also observed for At-*BOR1*, which itself has a close homolog (At-*BOR2*) (Miwa et al., 2013). The observation that both *Arabidopsis bor1* and maize *rte* mutants show strong recessive phenotypes despite the presence of closely related paralogs (Figure 5) suggests that BOR1/RTE proteins may be specialized to a certain degree. This finding is supported by the recent characterization of At-*BOR2*, which harbors unique root expression patterns and functions relative to At-*BOR1* (Miwa et al., 2013). Further examining the basis for the phenotypic specificity among closely related homologs in the same species may yield important information about the regulation of boron transport in plants and the relative contribution of each family member.

Boron Transport Is Required for the Structural Integrity of Cells in the Inflorescences

Boron is well known to be crucial for the cross-linking of the cell wall polysaccharide RG-II. Pectins, normally abundant in areas near growing and dividing cells, are critical constituents of the cell wall, play a role at the cell wall-plasma membrane interface and are crucial for organogenesis at the apical meristem (Hu et al., 1996; Kohorn, 2000; O'Neill et al., 2004; Mohnen, 2008; Hänsch and Mendel, 2009; Peaucelle et al., 2011). The high degree of evolutionary conservation of the RG-II/B structure suggests that it plays a fundamental role in cell wall structure and function (Matsunaga et al., 2004; Mohnen, 2008). Nutrient deficiencies and mutations that disrupt various aspects of RG-II/B dimer formation result in cellular changes such as the rapid decrease in the mechanical strength of the cell wall and severe growth defects (Mohnen, 2008; Camacho-Cristóbal et al., 2011). These phenotypes are evident in rapidly growing and reproductive tissues such as meristems, which are known to be more sensitive to boron deficiencies. For instance, the *Nicotiana plumbaginifolia GUT1* gene, responsible for the synthesis of the RG-II type pectin, was shown to be essential for intercellular attachment in normal meristem development as well as for floral organ formation and fertility (Iwai et al., 2002, 2006).

We hypothesized that the withered phenotype of *rte* ears likely results from insufficient boron supply to the rapidly growing meristematic tissue and developing organs, leading to inadequate levels of borate cross-linked RG-II and weakened cell walls. Consistent with this hypothesis, boron levels were indeed reduced in *rte* ears (Supplemental Figure 10), and TEM analysis of developing *rte* ears revealed that the cell and cell walls disintegrated during development (Figure 8). In particular, cell walls often swelled and lost their rigid structure, and this was accompanied by widespread cell death (Figures 8E to 8H). These findings are in agreement with those reported in pumpkin leaves, which showed that cell wall thickness varied based on boron availability and correlated with the levels of cross-linked RG-II/B dimers (Ishii et al., 2001). In another study, virus-induced gene silencing of a tobacco enzyme involved in RG-II cross-linking caused abnormal cell walls and eventually cell death in leaves (Ahn et al., 2006). Aberrant cell development and lignification were also observed in sections of leaf tissue of *rte* mutants (Supplemental Figure 2). Abnormalities in pectin network formation are known to alter the physical properties of the cell wall, such as increasing the size of cell wall pores and eventually causing ruptures (Fleischer et al., 1998, 1999; O'Neill et al., 2004). The production of reactive oxygen species and subsequent cell death has also been reported as an immediate downstream event of boron deprivation in cultured tobacco cells as well as in *Arabidopsis* roots. However, this appears to be a secondary effect associated with defective pectin cross-linking (Koshiba et al., 2009; Oiwa et al., 2013). We therefore propose that the lack of a proper cell wall structure caused by lower boron content results in cell expansion defects and eventually cell death in all inflorescence tissues, including meristems and floral organs.

Boron and Crop Productivity

Loss of productivity in crops due to deficient or toxic levels of boron in the soil has been reported in numerous crop species (Shorrocks, 1997; Dell and Huang, 1997) and continues to pose a major problem in many areas of the world. Several approaches have been developed in an attempt to translate the increased knowledge of boron transport into the generation of plants capable of growing in soils with adversely high boron content or in conditions of boron deficiency. Overexpression of *BOR1* in *Arabidopsis* increased boron translocation and seed yield under boron-limited conditions, demonstrating the potential to cultivate plants that can tolerate low boron supply (Miwa et al., 2006). On the other hand, overexpression of *BOR4* resulted in improved growth under toxic levels of boron (Miwa et al., 2007). In barley, a quantitative trait locus study to identify genetic factors regulating tolerance to toxic levels of boron revealed an African landrace with multiple copies of the *Bot1* gene. *Bot1* encodes a BOR4 homolog (Takano et al., 2008), whose expression is higher in the tolerant landrace, suggesting increased export of boron from the cells to the apoplast (Sutton et al., 2007; Miwa and Fujiwara, 2010). Similarly, wheat varieties tolerant to high boron levels showed higher expression of *BOR* homologs (Reid, 2007). Expanding our understanding of the molecular mechanisms of boron transport in crop species is

a crucial step for designing strategies for biotechnological application to improve yields and create alternatives to chemical fertilization in regions where poor soil quality is a major problem.

METHODS

Plant Materials and Phenotypic Analysis

rte mutants were originally identified in mutagenized populations created by the Maize Inflorescence Project (http://www.maizegdb.org/ems-phenotype.php). Seeds corresponding to stock numbers 04HI-Mo17XA632GN-16, 04HI-Mo17xA632GN-128, 04HI-Mo17xA632GN-157 (*rte-1*; see below), 04HI-OH43xA632GN-190 (*rte-2*), and 04HI-A632TR-97 (*rte-3*) were provided by the Maize Genetics Cooperation Stock Center. A fourth allele, *rte-4*, was identified in a different EMS-mutagenized population fixed for the *ramosa2-R* mutation (Bortiri et al., 2006) in the inbred line A619.

For phenotypic analysis, tassel measurements were taken after two rounds of backcrossing of *rte-1* with the inbred line Mo17. Tassel length was measured as the distance from the first tassel branch to the tassel tip, while branch length was determined by the four longest branches of tassels. Branches were defined as having more than two spikelets. Student's *t* test was used to determine statistical significance. Figure 1D shows *rte-1* backcrossed three times in A619. The *rte-1* allele backcrossed once to Mo17 was used for the boron rescue experiment and for phenotypic comparison at different field locations.

To assess pollen viability, freshly collected pollen grains were germinated on plates (10% sucrose, 0.0025% H_3BO_3, 20 mM $CaCl_2$, 0.05 mM KH_2PO_4, 6% polyethylene glycol 4000, and 0.3% noble agar). After 30 to 60 min incubation at room temperature, pictures were taken using a Leica M205C stereomicroscope.

Positional Cloning of the *rte* Mutant

For preliminary mapping, pools of 31 to 40 mutant and wild-type samples from individual *rte* alleles were collected from M3 mapping populations. DNA extracted from the pooled samples was sent to the Genomic Technologies Facility at Iowa State University to be analyzed via bulk segregant analysis using the MassARRAY system (Sequenom) (Liu et al., 2010). For positional cloning, SSR markers were selected from MaizeGDB (http://www.maizegdb.org), and new molecular markers were developed based on available genome sequence information (Supplemental Table 1). Shortly after mapping efforts were initiated, it became apparent that the causative *rte* mutation present in stocks 04HI-Mo17XA632GN-16, 04HI-Mo17xA632GN-128, and 04HI-Mo17xA632GN-157 occurred in the wild-type Mo17 background that was used as a recipient of the EMS-mutagenized pollen. Subsequent analysis showed that these three alleles possessed identical lesions in the *rte* locus. Therefore, we designated 04HI-Mo17XA632GN-16, 04HI-Mo17xA632GN-128, and 04HI-Mo17xA632GN-157 as *rte-1*.

The *Sorghum bicolor* genome sequence (http://www.phytozome.org) was used to identify putative candidate genes in our mapping window (Paterson et al., 2009). Corresponding maize (*Zea mays*) genomic sequences were obtained by MAGI and NCBI BLAST database searches. Newly developed markers and primers used for genotyping *rte-1* and *rte*-2 alleles are listed in Supplemental Table 1. The genomic region containing the *rte* gene was sequenced using primers RTE-F1/RTE-R1, RTE-F2/RTE-R2, and RTE-F3/RTE-R3 (Supplemental Table 1). To clone the *rte* full-length coding sequence, we generated two overlapping cDNA fragments of *rte*, using primers RTE-cds-F1 and RTE-cds-R3, and primers RTE-cds-F3 and RTE-cds-R2 (Supplemental Table 1) using B73 RNA as template. The two fragments were subsequently joined by PCR. The complete *rte* coding sequences was then A-tailed and cloned into the pGEM-T Easy vector system (Promega).

Scanning and Transmission Electron Microscopy

For scanning electron microscopy, samples were fixed with 4% paraformaldehyde in PBS buffer at 4°C for 36 h. Subsequently, the samples were rinsed with 130 mM NaCl followed by dehydration through a graded ethanol series up to 100% ethanol and dried using a CPD 020 Balzers critical point dryer. Once dried, the samples were mounted onto adhesive-coated aluminum stubs, sputter coated with palladium/gold alloy with help of SCD004 Balzers sputter coater, and imaged using an Amray 1830 I scanning electron microscope.

For TEM, the samples were fixed in 2.5% glutaraldehyde in 0.1 M sodium cacodylate buffer, pH 7.4, containing 2% sucrose for 2 h. Postfixation was performed in 1% osmium tetroxide in the same buffer for 1.5 h followed by dehydration in a graded ethanol series and embedded in Spurr's Low Viscosity Embedding media. Thin sections taken from 2 mm below the ear tip were prepared using a diamond knife and Ultracut E ultramicrotome (Reichert Optische Werke). Sections were stained with 5% uranyl acetate saturated solution in 50% ethanol for 15 min and then with 0.5% lead citrate solution in CO_2-free double-distilled water (Reynold's Lead Citrate Stain) for 2 min. Observation and micrographs were made with a JEM-100CXII electron microscope (JEOL).

Histology and Microscopy

Histological sections of maize ears were stained with Toluidine blue, and leaf sections were stained with Saffranin O and Alcian Blue as previously described (Gallavotti et al., 2011) and visualized with a Leica DM5500B microscope. Confocal laser scanning microscopy was performed on a Leica SP5 confocal microscope using 514-nm excitation and 520- to 575-nm emission. Image processing was performed with ImageJ.

Sequence Analysis and Phylogenetic Tree Construction

Comparative sequence analysis was performed with NCBI BLAST and ClustalW2. For phylogenetic analysis, 94 *rte*-like genes were identified through searches at Phytozome (http://www.phytozome.org). The distantly related *Chlamydomonas reinhardtii* BOR1-like protein was used as outgroup. The nucleotide sequence alignment was assembled and translated into amino acid sequences using Mesquite (http://mesquiteproject.org), aligned using MUSCLE (Edgar, 2004), then manually adjusted using Mesquite. Bayesian phylogenetic analyses using MrBayes 3.2 (Ronquist and Huelsenbeck, 2003) on the Grethor parallel processing cluster at the University of Missouri St. Louis consisted of two separate searches of 10 million generations using flat priors and the General Time Reversible (GTR) model of sequence evolution, invariant sites, and gamma distributed rates partitioned according to codon position (GTR + I + SS) and with trees being sampled every 1000 generations. Convergence between the two runs was determined by examining the average SD of the split frequencies (0.006077). After convergence had been assured the first 25% of trees were removed as burn-in and clade credibility values estimated using MrBayes.

Boron Measurements

Inductively coupled plasma optical emission spectroscopy was used to measure boron levels by the Missouri University Plant and Soil Analysis Facility. For measuring leaf and ear boron content, the uppermost three leaves and the first and second ears (2 to 5 cm) from wild-type and *rte* mutant plants were bulked from at least three plants grown in the winter nursery in Molokai.

Expression Analysis

Total RNA was extracted from different tissues obtained from pools of three or more B73 plants using standard procedures. These include embryos and endosperm at 10 d after pollination, mature leaf blades, seedlings, roots,

and tassel and ear at 0.2 and 0.6 cm stages. cDNA was obtained using the qScript cDNA Synthesis kit and amplified with PerfeCTa SYBR Green FastMix (Quanta Biosciences). For tissue-specific expression, real-time PCR was performed using primer pairs *rte-RT* for the *rte* gene and *ubi-RT* for *ubiquitin* as a control (Supplemental Table 1). The CT (cycle threshold) values for all genes in different RNA samples were normalized to the CT value of the internal control gene. Relative mRNA levels for each gene in different tissue samples were calculated using the ΔΔCT method (StepOnePlus real-time PCR system; Applied Biosystems).

For in situ hybridization, the full-length *rte* cDNA was cloned into pGEM-T Easy vector system (Promega) using *rte-CDS* primers (Supplemental Table 1). PCR products obtained using primers M13F and M13R primer were used as templates for synthesizing sense and antisense RNA probes. T7 and SP6 RNA polymerases were used for in vitro transcription using the DIG RNA labeling kit (Roche Diagnostics). Experimental procedures were previously described (Gallavotti et al., 2011).

Complementation Test and Transient Expression Assay

To create the $35S_{pro}$*:rte* construct for complementation of the *bor1-3* mutant, the *rte* coding sequence was amplified with Phusion polymerase using primers RTE-35s/pBJ36-XhoI-F1 and RTE-35s/pBJ36-XhoI-R1 (Supplemental Table 1). The amplicon was subsequently cloned into the *Xho*I site of pBJ36+2x35S using Cold Fusion technology (System Biosciences). The $35S_{pro}$*:rte* cassette was isolated using *Not*I digestion and shuttled into the binary vector pMLBART. The $35S_{pro}$*:rte-L361* mutated version was created by changing the TCA codon (serine) to TTA (leucine) using primers RTE793-Nco-F and RTE1195-Leu-R, and RTE1069-Leu-F and RTE2103-Stu-R (Supplemental Table 1). The resulting amplicons were inserted into the *Nco*I and *Stu*I sites of *pBJ36+2x35S-rte* using Gibson Assembly. The $35S_{pro}$*:rte-L361* cassette was subsequently isolated using *Not*I digestion and shuttled into the binary vector pMLBART.

The *bor1-3* mutant (Kasai et al., 2011) corresponding to T-DNA line SALK_037312 (Alonso et al., 2003) was obtained from the ABRC. Homozygous *bor1-3* lines were selected by PCR amplification with primers BOR1-037312-R and LBb1.3, and BOR1-037312-F and BOR1-037312-R, propagated by irrigation with 150 μM boric acid and transformed by the floral dip method (Clough and Bent, 1998). Primary transformants containing the $35S_{pro}$*:rte* construct were Basta-selected on soil without supplemental boron (Promix Biofungicide Professional Growing Medium), genotyped to confirm the presence of the homozygous *bor1-3* T-DNA insertion, and assessed for phenotypic rescue of *bor1* defects. Wild-type Columbia-0 plants were used as controls.

To create the $35S_{pro}$*:rte:YFP* and $35S_{pro}$*:rte-L361:YFP* constructs for transient expression in tobacco (*Nicotiana tabacum*), the *rte* coding sequence (without stop codon) was PCR amplified with primers RTE-pENTR-SFI-F and RTE-pENTR-SFI-R from templates *pBJ36+2x35*S_{pro}*:rte* and *pBJ36+2x35*S_{pro}*:rte-L361*, respectively. Resulting fragments were directionally cloned into the *Sfi*I sites of pENTRsfi-223.1 using standard cloning procedures. The resulting *pENTR-rte* and *pENTR-rte-L361* constructs were Gateway recombined using LR clonase into pEarlyGate101 (Earley et al., 2006). pEarlyGate104 containing a $35S_{pro}$*:YFP* cassette with the ccdB cassette removed was used as a YFP only control. The corresponding *Agrobacterium tumefaciens* tobacco leaf infection was performed as described previously (Gallavotti et al., 2011).

Boric Acid Rescue and Soil Analysis

All maize plants were grown in standard greenhouse conditions in pots with soil supplemented with 20 g of Osmocote Classic. Six homozygous and heterozygous *rte* plants were grown for each treatment. Upon germination, the irrigation water was supplemented with boric acid at different concentrations until harvesting. Field soil samples were collected from the area located near *rte* plants according to standard practices and analyzed at the New Jersey Agricultural Experiment Station, Rutgers University.

Accession Numbers

Sequence data from this article can be found in the MaizeGDB database under the following ID numbers: *GRMZM2G166159_T01* (*rte*), *GRMZM2G082203_T01* (*rte2*), and *GRMZM2G047732_T01* (*ubi*).

Supplemental Data

The following materials are available in the online version of this article.

Supplemental Figure 1. Additional Phenotypes of *rte-1* and *rte-2* Mutants.

Supplemental Figure 2. *rte* Leaf Sections.

Supplemental Figure 3. Histological Analysis of *rte* Reproductive Development.

Supplemental Figure 4. In Situ Hybridizations of *rte-1* Ears Probed with the Meristem Marker *knotted1* (*kn1*).

Supplemental Figure 5. The Tassel and Ear Phenotype of *rte-3* and *rte-4*.

Supplemental Figure 6. Protein Sequence Alignment of BOR1 Homologs in Different Species.

Supplemental Figure 7. Rescue of the *rte-1* Tassel Phenotype.

Supplemental Figure 8. Quantification of the Rescue of the *rte-1* Tassel Phenotype.

Supplemental Figure 9. The *rte* Phenotype Is Influenced by the Boron Concentration in the Soil.

Supplemental Figure 10. Boron Measurements in *rte* Mutants.

Supplemental Figure 11. Tissue-Specific Expression Data of *rte*.

Supplemental Table 1. List of Primers Used.

Supplemental Data Set 1. Nexus File Used for the Phylogenetic Analysis.

ACKNOWLEDGMENTS

We thank Valentin Starovoytov for assistance with scanning electron microscopy and TEM; Marty Sachs and the Maize Genetics Cooperation Stock Center for providing the seeds containing all *rte* alleles; the Maize Inflorescence Project for generating EMS populations; ABRC for T-DNA insertion lines; Marc Probasco for help with field preparation and greenhouse management at Rutgers University; Lu Gao and Pat Schnable for bulk segregant analysis; Paula McSteen, Amanda Durbak, and Kim Phillips for the bulk segregant analysis of family 04HI-Mo17xA632GN-128 and B measurements; the University of Missouri-St. Louis for access to the Grethor parallel processing cluster; and Robert Schmidt for helpful comments. We acknowledge funding from the National Science Foundation (IOS-0820729/IOS-1114484) to A.G. and S.M. and from the Waksman Institute to A.G. Some of this material is based upon work by S.M., while serving at the National Science Foundation. Any opinion, findings, and conclusions or recommendations expressed in this material are those of the authors and do not necessarily reflect the views of the National Science Foundation.

AUTHOR CONTRIBUTIONS

M.C., Z.T., M.G., S.M., A.B., M.M., and A.G. performed experiments. M.C., M.G., S.M., M.M., and A.G. designed the research. M.C., Z.T., M.G., S.M., M.M., and A.G. analyzed the data. M.C., Z.T., M.G., S.M., M.M., and A.G. wrote the article.

Received April 3, 2014; revised June 2, 2014; accepted June 23, 2014; published July 17, 2014.

REFERENCES

Ahn, J.W., Verma, R., Kim, M., Lee, J.Y., Kim, Y.K., Bang, J.W., Reiter, W.D., and Pai, H.S. (2006). Depletion of UDP-D-apiose/UDP-D-xylose synthases results in rhamnogalacturonan-II deficiency, cell wall thickening, and cell death in higher plants. J. Biol. Chem. **281:** 13708–13716.

Alassimone, J., Naseer, S., and Geldner, N. (2010). A developmental framework for endodermal differentiation and polarity. Proc. Natl. Acad. Sci. USA **107:** 5214–5219.

Alonso, J.M., et al. (2003). Genome-wide insertional mutagenesis of *Arabidopsis thaliana*. Science **301:** 653–657.

Argust, P. (1998). Distribution of boron in the environment. Biol. Trace Elem. Res. **66:** 131–143.

Baxter, I. (2009). Ionomics: studying the social network of mineral nutrients. Curr. Opin. Plant Biol. **12:** 381–386.

Bortiri, E., Chuck, G., Vollbrecht, E., Rocheford, T., Martienssen, R., and Hake, S. (2006). ramosa2 encodes a LATERAL ORGAN BOUNDARY domain protein that determines the fate of stem cells in branch meristems of maize. Plant Cell **18:** 574–585.

Braybrook, S.A., and Peaucelle, A. (2013). Mechano-chemical aspects of organ formation in *Arabidopsis thaliana*: the relationship between auxin and pectin. PLoS ONE **8:** e57813.

Caffall, K.H., and Mohnen, D. (2009). The structure, function, and biosynthesis of plant cell wall pectic polysaccharides. Carbohydr. Res. **344:** 1879–1900.

Camacho-Cristóbal, J.J., Rexach, J., Herrera-Rodríguez, M.B., Navarro-Gochicoa, M.T., and González-Fontes, A. (2011). Boron deficiency and transcript level changes. Plant Sci. **181:** 85–89.

Chen, X., Schauder, S., Potier, N., Van Dorsselaer, A., Pelczer, I., Bassler, B.L., and Hughson, F.M. (2002). Structural identification of a bacterial quorum-sensing signal containing boron. Nature **415:** 545–549.

Chormova, D., Messenger, D.J., and Fry, S.C. (2014). Boron bridging of rhamnogalacturonan-II, monitored by gel electrophoresis, occurs during polysaccharide synthesis and secretion but not post-secretion. Plant J. **77:** 534–546.

Clough, S.J., and Bent, A.F. (1998). Floral dip: a simplified method for Agrobacterium-mediated transformation of *Arabidopsis thaliana*. Plant J. **16:** 735–743.

Dell, B., and Huang, L.B. (1997). Physiological response of plants to low boron. Plant Soil **193:** 103–120.

Domagalska, M.A., and Leyser, O. (2011). Signal integration in the control of shoot branching. Nat. Rev. Mol. Cell Biol. **12:** 211–221.

Earley, K.W., Haag, J.R., Pontes, O., Opper, K., Juehne, T., Song, K., and Pikaard, C.S. (2006). Gateway-compatible vectors for plant functional genomics and proteomics. Plant J. **45:** 616–629.

Edgar, R.C. (2004). MUSCLE: a multiple sequence alignment method with reduced time and space complexity. BMC Bioinformatics **5:** 113.

Eltinge, E.T. (1936). Effect of boron deficiency upon the structure of *Zea mays*. Plant Physiol. **11:** 765–778.

Findeklee, P., and Goldbach, H.E. (1996). Rapid effects of boron deficiency on cell wall elasticity modulus in *Cucurbita pepo* roots. Bot. Acta **109:** 463–465.

Fleischer, A., Titel, C., and Ehwald, R. (1998). The boron requirement and cell wall properties of growing and stationary suspension-cultured *chenopodium album* L. cells. Plant Physiol. **117:** 1401–1410.

Fleischer, A., O'Neill, M.A., and Ehwald, R. (1999). The pore size of non-graminaceous plant cell walls is rapidly decreased by borate ester cross-linking of the pectic polysaccharide rhamnogalacturonan II. Plant Physiol. **121:** 829–838.

Fort, D.J. (2002). Boron deficiency disables *Xenopus laevis* oocyte maturation events. Biol. Trace Elem. Res. **85:** 157–169.

Gallavotti, A., Malcomber, S., Gaines, C., Stanfield, S., Whipple, C., Kellogg, E., and Schmidt, R.J. (2011). BARREN STALK FASTIGIATE1 is an AT-hook protein required for the formation of maize ears. Plant Cell **23:** 1756–1771.

Hänsch, R., and Mendel, R.R. (2009). Physiological functions of mineral micronutrients (Cu, Zn, Mn, Fe, Ni, Mo, B, Cl). Curr. Opin. Plant Biol. **12:** 259–266.

Hu, H.N., Brown, P.H., and Labavitch, J.M. (1996). Species variability in boron requirement is correlated with cell wall pectin. J. Exp. Bot. **47:** 227–232.

Huang, F., Zago, M.K., Abas, L., van Marion, A., Galván-Ampudia, C.S., and Offringa, R. (2010). Phosphorylation of conserved PIN motifs directs Arabidopsis PIN1 polarity and auxin transport. Plant Cell **22:** 1129–1142.

Huang, L.B., Pant, J., Dell, B., and Bell, R.W. (2000). Effects of boron deficiency on anther development and floret fertility in wheat (*Triticum aestivum* L-'Wilgoyne'). Ann. Bot. (Lond.) **85:** 493–500.

Ishii, T., Matsunaga, T., and Hayashi, N. (2001). Formation of rhamnogalacturonan II-borate dimer in pectin determines cell wall thickness of pumpkin tissue. Plant Physiol. **126:** 1698–1705.

Iwai, H., Masaoka, N., Ishii, T., and Satoh, N. (2002) A pectin glucuronyltransferase gene is essential for intercellular attachment in the plant meristem. Proc. Natl. Acad. Sci. USA **99:** 16319–16324.

Iwai, H., Hokura, A., Oishi, M., Chida, H., Ishii, T., Sakai, S., and Satoh, S. (2006). The gene responsible for borate cross-linking of pectin Rhamnogalacturonan-II is required for plant reproductive tissue development and fertilization. Proc. Natl. Acad. Sci. USA **103:** 16592–16597.

Jackson, D., Veit, B., and Hake, S. (1994). Expression of maize Knotted1 related homeobox genes in the shoot apical meristem predicts patterns of morphogenesis in the vegetative shoot. Development **120:** 405–413.

Kasai, K., Takano, J., Miwa, K., Toyoda, A., and Fujiwara, T. (2011). High boron-induced ubiquitination regulates vacuolar sorting of the BOR1 borate transporter in *Arabidopsis thaliana*. J. Biol. Chem. **286:** 6175–6183.

Kobayashi, M., Matoh, T., and Azuma, J. (1996). Two chains of rhamnogalacturonan II are cross-linked by borate-diol ester bonds in higher plant cell walls. Plant Physiol. **110:** 1017–1020.

Kohorn, B.D. (2000). Plasma membrane-cell wall contacts. Plant Physiol. **124:** 31–38.

Koshiba, T., Kobayashi, M., and Matoh, T. (2009). Boron nutrition of tobacco BY-2 cells. V. oxidative damage is the major cause of cell death induced by boron deprivation. Plant Cell Physiol. **50:** 26–36.

Lanoue, L., Taubeneck, M.W., Muniz, J., Hanna, L.A., Strong, P.L., Murray, F.J., Nielsen, F.H., Hunt, C.D., and Keen, C.L. (1998). Assessing the effects of low boron diets on embryonic and fetal development in rodents using in vitro and in vivo model systems. Biol. Trace Elem. Res. **66:** 271–298.

Liu, S., Chen, H.D., Makarevitch, I., Shirmer, R., Emrich, S.J., Dietrich, C.R., Barbazuk, W.B., Springer, N.M., and Schnable, P.S. (2010). High-throughput genetic mapping of mutants via quantitative single nucleotide polymorphism typing. Genetics **184:** 19–26.

Loomis, W.D., and Durst, R.W. (1992). Chemistry and biology of boron. Biofactors **3:** 229–239.

Lordkaew, S., Dell, B., Jamjod, S., and Rerkasem, B. (2011). Boron deficiency in maize. Plant Soil **342:** 207–220.

Matsunaga, T., Ishii, T., Matsumoto, S., Higuchi, M., Darvill, A., Albersheim, P., and O'Neill, M.A. (2004). Occurrence of the primary cell wall polysaccharide rhamnogalacturonan II in pteridophytes, lycophytes, and bryophytes. Implications for the evolution of vascular plants. Plant Physiol. **134:** 339–351.

McSteen, P., Laudencia-Chingcuanco, D., and Colasanti, J. (2000). A floret by any other name: control of meristem identity in maize. Trends Plant Sci. **5:** 61–66.

Miwa, K., Takano, J., and Fujiwara, T. (2006). Improvement of seed yields under boron-limiting conditions through overexpression of

BOR1, a boron transporter for xylem loading, in *Arabidopsis thaliana*. Plant J. **46:** 1084–1091.

Miwa, K., Takano, J., Omori, H., Seki, M., Shinozaki, K., and Fujiwara, T. (2007). Plants tolerant of high boron levels. Science **318:** 1417.

Miwa, K., and Fujiwara, T. (2010). Boron transport in plants: co-ordinated regulation of transporters. Ann. Bot. (Lond.) **105:** 1103–1108.

Miwa, K., Wakuta, S., Takada, S., Ide, K., Takano, J., Naito, S., Omori, H., Matsunaga, T., and Fujiwara, T. (2013). Roles of BOR2, a boron exporter, in cross linking of rhamnogalacturonan II and root elongation under boron limitation in Arabidopsis. Plant Physiol. **163:** 1699–1709.

Mohnen, D. (2008). Pectin structure and biosynthesis. Curr. Opin. Plant Biol. **11:** 266–277.

Nakagawa, Y., Hanaoka, H., Kobayashi, M., Miyoshi, K., Miwa, K., and Fujiwara, T. (2007). Cell-type specificity of the expression of Os BOR1, a rice efflux boron transporter gene, is regulated in response to boron availability for efficient boron uptake and xylem loading. Plant Cell **19:** 2624–2635.

Noguchi, K., Yasumori, M., Imai, T., Naito, S., Matsunaga, T., Oda, H., Hayashi, H., Chino, M., and Fujiwara, T. (1997). bor1-1, an *Arabidopsis thaliana* mutant that requires a high level of boron. Plant Physiol. **115:** 901–906.

Noguchi, K., Ishii, T., Matsunaga, T., Kakegawa, K., Hayashi, H., and Fujiwara, T. (2003). Biochemical properties of the cell wall in the Arabidopsis mutant bor1-1 in relation to boron nutrition. J. Plant Nutr. Soil Sci. **166:** 175–178.

Oiwa, Y., Kitayam, K., Kobayashi, M., and Matoh, T. (2013). Boron deprivation immediately causes cell death in growing roots of Arabidopsis thaliana (L.) Heynh. Soil Sci. Plant Nutr. **59:** 621–627.

O'Neill, M.A., Eberhard, S., Albersheim, P., and Darvill, A.G. (2001). Requirement of borate cross-linking of cell wall rhamnogalacturonan II for Arabidopsis growth. Science **294:** 846–849.

O'Neill, M.A., Ishii, T., Albersheim, P., and Darvill, A.G. (2004). Rhamnogalacturonan II: structure and function of a borate cross-linked cell wall pectic polysaccharide. Annu. Rev. Plant Biol. **55:** 109–139.

Paterson, A.H., et al. (2009). The *Sorghum bicolor* genome and the diversification of grasses. Nature **457:** 551–556.

Peaucelle, A., Braybrook, S.A., Le Guillou, L., Bron, E., Kuhlemeier, C., and Höfte, H. (2011). Pectin-induced changes in cell wall mechanics underlie organ initiation in Arabidopsis. Curr. Biol. **21:** 1720–1726.

Pérez-Castro, R., Kasai, K., Gainza-Cortés, F., Ruiz-Lara, S., Casaretto, J.A., Peña-Cortés, H., Tapia, J., Fujiwara, T., and González, E. (2012). VvBOR1, the grapevine ortholog of AtBOR1, encodes an efflux boron transporter that is differentially expressed throughout reproductive development of *Vitis vinifera* L. Plant Cell Physiol. **53:** 485–494.

Reid, R. (2007). Identification of boron transporter genes likely to be responsible for tolerance to boron toxicity in wheat and barley. Plant Cell Physiol. **48:** 1673–1678.

Ronquist, F., and Huelsenbeck, J.P. (2003). MrBayes 3: Bayesian phylogenetic inference under mixed models. Bioinformatics **19:** 1572–1574.

Roppolo, D., De Rybel, B., Tendon, V.D., Pfister, A., Alassimone, J., Vermeer, J.E., Yamazaki, M., Stierhof, Y.D., Beeckman, T., and Geldner, N. (2011). A novel protein family mediates Casparian strip formation in the endodermis. Nature **473:** 380–383.

Rowe, R.I., and Eckhert, C.D. (1999). Boron is required for zebrafish embryogenesis. J. Exp. Biol. **202:** 1649–1654.

Shorrocks, V.M. (1997). The occurrence and correction of boron deficiency. Plant Soil **193:** 121–148.

Sutton, T., Baumann, U., Hayes, J., Collins, N.C., Shi, B.J., Schnurbusch, T., Hay, A., Mayo, G., Pallotta, M., Tester, M., and Langridge, P. (2007). Boron-toxicity tolerance in barley arising from efflux transporter amplification. Science **318:** 1446–1449.

Takano, J., Miwa, K., and Fujiwara, T. (2008). Boron transport mechanisms: collaboration of channels and transporters. Trends Plant Sci. **13:** 451–457.

Takano, J., Miwa, K., Yuan, L., von Wirén, N., and Fujiwara, T. (2005). Endocytosis and degradation of BOR1, a boron transporter of *Arabidopsis thaliana*, regulated by boron availability. Proc. Natl. Acad. Sci. USA **102:** 12276–12281.

Takano, J., Noguchi, K., Yasumori, M., Kobayashi, M., Gajdos, Z., Miwa, K., Hayashi, H., Yoneyama, T., and Fujiwara, T. (2002). Arabidopsis boron transporter for xylem loading. Nature **420:** 337–340.

Takano, J., Tanaka, M., Toyoda, A., Miwa, K., Kasai, K., Fuji, K., Onouchi, H., Naito, S., and Fujiwara, T. (2010). Polar localization and degradation of Arabidopsis boron transporters through distinct trafficking pathways. Proc. Natl. Acad. Sci. USA **107:** 5220–5225.

Takano, J., Wada, M., Ludewig, U., Schaaf, G., von Wirén, N., and Fujiwara, T. (2006). The Arabidopsis major intrinsic protein NIP5;1 is essential for efficient boron uptake and plant development under boron limitation. Plant Cell **18:** 1498–1509.

Takano, J., Yamagami, M., Noguchi, K., Hayashi, H., and Fujiwara, T. (2001). Preferential translocation of boron to young leaves in *Arabidopsis thaliana* regulated by the BOR1 gene. Soil Sci. Plant Nutr. **47:** 345–357.

Tanaka, M., Wallace, I.S., Takano, J., Roberts, D.M., and Fujiwara, T. (2008). NIP6;1 is a boric acid channel for preferential transport of boron to growing shoot tissues in Arabidopsis. Plant Cell **20:** 2860–2875.

Wimmer, M.A., and Eichert, T. (2013). Review: mechanisms for boron deficiency-mediated changes in plant water relations. Plant Sci. **203-204:** 25–32.

Wimmer, M.A., Lochnit, G., Bassil, E., Mühling, K.H., and Goldbach, H.E. (2009). Membrane-associated, boron-interacting proteins isolated by boronate affinity chromatography. Plant Cell Physiol. **50:** 1292–1304.

Yoshinari, A., Kasai, K., Fujiwara, T., Naito, S., and Takano, J. (2012). Polar localization and endocytic degradation of a boron transporter, BOR1, is dependent on specific tyrosine residues. Plant Signal. Behav. **7:** 46–49.